Nonlinear Theory of the Internally Loss-Modulated Laser

ODIS P. McDUFF, SENIOR MEMBER, IEEE AND STEPHEN E. HARRIS, MEMBER, IEEE

Abstract—**This paper presents a detailed nonlinear analysis of the internally loss-modulated laser including the effect of arbitrary atomic lineshape, saturation, and mode pulling. Results of the analysis are in part numerical and include a study of the spectral and time domain behavior of the laser output. The results include a determination of the minimum perturbation strength which is necessary to produce phase locking, peak pulse amplitude, and minimum pulsewidth as a function of perturbation strength, a consideration of the detuned case, and a comparison of AM- versus FM-type phase locking. Results are compared with the previously obtained linearized solutions of others.**

I. Introduction

PHASE LOCKING of the optical modes of a gas laser by means of internal loss modulation was first reported by Hargrove, Fork, and Pollack.[1] Theoretical studies have been given by DiDomenico,[2] Yariv,[3] and Crowell,[4] who present solutions for a linearized approximation to the problem. Experimental results on helium–neon and argon lasers have been given by Crowell.[4] Deutsch[5] reported phase locking of a ruby laser and Pantell and Kohn[6] have presented a linearized transient study of the ruby laser. Recently, DiDomenico et al.[7] have reported phase locking of a YAlG:Nd laser.

In this paper we present a detailed study of AM-type mode locking which includes the effects of atomic lineshape, saturation, and frequency pulling. The results of this nonlinear study differ appreciably from those of the earlier linear theories. In particular, the modulator drive strength becomes an important parameter in determining the characteristics of the pulsing laser.

The techniques employed and the form of the present paper are similar to those of a previous paper.[9] In the following sections, we first derive and discuss the equations which govern AM-type locking. Conservation conditions are derived and the equations are put into what, in effect, is an integral form, useful in later sections. Numerical results which show the effect of varying the modulator drive strength and frequency are given. It will be seen that at low modulator levels mode phases depart considerably from their ideal values with the result that the laser pulses may have sidelobes of appreciable magnitude. Curves of peak pulse intensity, and pulsewidth versus modulator drive strength are given. Later sections of the paper consider the question of threshold for locking and study the problem of phase locking a laser where only a single mode has gain. It will be seen that, in principle, the pulsewidth in such a laser may be made as small as that of a multimode laser.

Before proceeding we note that periodic pulsing of a laser may also be obtained by means of an internal phase perturbation which is driven at a frequency equal to that of the axial mode interval.[8] Studies of this process have been given by Harris and McDuff[9] and by Ammann, McMurtry, and Oshman.[10] Except for occasional comparisons, this type of locking will not be considered in the present paper.

II. Basic Differential Equations

In this section we summarize the derivation of the coupled-mode differential equations. The procedure is basically the same as that used in an earlier paper on the FM laser.[9]

We start with the self-consistency equations of Lamb[11] which describe the effect of an arbitrary optical polarization upon the electric fields of a high-Q optical resonator. In the present case, the polarization includes a contribution resulting from the inverted atomic media and a parametric contribution resulting from the loss perturbation. We assume the loss perturbation to be represented by a quadrature component of susceptibility,

$$\Delta\chi''(z, t) = \Delta\chi''(z)[1 + \cos \nu_m t], \tag{1}$$

where ν_m is the driving frequency of the perturbation and is approximately equal to $\Delta\Omega$, the frequency separation of the resonances Ω_n of the empty optical cavity.[1] The parametric contribution to total polarization is then

$$P_{\text{Parametric}}(z, t) = \sum_n \epsilon_0 \, \Delta\chi''(z, t) E_n(t) \sin [\nu_n t + \varphi_n(t)] U_n(z) \tag{2}$$

where

$$U_n(z) = \sin (n_0 + n)\pi z/L,$$

and the total cavity electromagnetic field has been expanded in the form[2]

$$E(z, t) = \sum_n E_n(t) \cos [\nu_n t + \varphi_n(t)] U_n(z).$$

Here $E_n(t)$ and $\varphi_n(t)$ are the slowly time-varying amplitude and phase of the nth mode, ν_n is its frequency, and L is the cavity length. We define

$$\alpha_a = \frac{2\nu}{c} \int_0^L \Delta\chi''(z) U_n^2(z) \, dz \tag{3}$$

Manuscript received July 8, 1966; revised December 1, 1966. The work reported in this paper was sponsored by the National Aeronautics and Space Administration under NASA Grant NGR-05-020-103. O. P. McDuff was supported in part by a National Science Foundation Faculty Fellowship.

O. P. McDuff is with the Department of Electrical Engineering, University of Alabama, University, Ala. He was formerly with Stanford University.

S. E. Harris is with Stanford University, Stanford, Calif.

[1] We adopt the convention that all symbols for frequency shall denote circular frequencies.

[2] Except where noted, all sums will be from $-\infty$ to $+\infty$.

and

$$\alpha_c = \frac{\nu}{c}\int_0^L \Delta\chi''(z)U_{n\pm1}(z)U_n(z). \tag{4}$$

The parametric component of polarization driving the nth mode is given by

$$P_n(t) = \frac{2}{L}\int_0^L P(z, t)U_n(z)\,dz,$$

which becomes upon combining (1) through (4) and assuming that only adjacent mode coupling applies,

$$\begin{aligned} P_n(t) = {} & \frac{\epsilon_0\alpha_a c}{\nu L}E_n \sin(\nu_n t + \varphi_n) + \frac{\epsilon_0\alpha_c c}{\nu L}[E_{n+1}\cos(\varphi_{n+1} - \varphi_n) \\ & + E_{n-1}\cos(\varphi_n - \varphi_{n-1})]\sin(\nu_n t + \varphi_n) \\ & + \frac{\epsilon_0\alpha_c c}{\nu L}[E_{n+1}\sin(\varphi_{n+1} - \varphi_n) \\ & - E_{n-1}\sin(\varphi_n - \varphi_{n-1})]\cos(\nu_n t + \varphi_n). \end{aligned} \tag{5}$$

We include the contribution of the atomic medium to the polarization by macroscopic quadrature and in phase components of susceptibility χ_n'' and χ_n', respectively. The nonlinear effects of the medium are included in the χ_n'' and χ_n'. The self-consistency equations then become

$$\begin{aligned} & [\dot{\varphi}_n - n\,\Delta\nu + \tfrac{1}{2}\nu\chi_n']E_n \\ & = -\frac{\alpha_c c}{2L}[E_{n+1}\sin(\varphi_{n+1} - \varphi_n) - E_{n-1}\sin(\varphi_n - \varphi_{n-1})] \end{aligned} \tag{6}$$

and

$$\begin{aligned} \dot{E}_n + \frac{\nu}{2}\left[\frac{1}{Q_n} + \chi_n''\right]E_n = {} & -\frac{\alpha_a c}{2L}E_n - \frac{\alpha_c c}{2L} \\ & \cdot[E_{n+1}\cos(\varphi_{n+1} - \varphi_n) + E_{n-1}\cos(\varphi_n - \varphi_{n-1})], \end{aligned} \tag{7}$$

where we have taken $\Delta\nu$ to be the detuning of the driving frequency from the axial mode interval $\Delta\Omega$, i.e.,

$$\Omega_n - \nu_n = n\,\Delta\nu. \tag{8}$$

Equations (6) and (7) are the basic differential equations to be considered and when solved give the amplitude, frequency, and phase of the optical modes. They can be combined to give a set of complex coupled-mode equations as presented by DiDomenico,[2] Yariv,[3] and Crowell.[4] The retention of the $\dot{\varphi}_n$ term (which is implicit in Yariv's equations but assumed zero in DiDomenico's and Crowell's) facilitates the inclusion of pulling and pushing of the entire coupled-mode oscillation.

III. Discussion of Parameters

Assuming small gain, we relate the small-signal saturated single-pass power gain to the quadrature component of susceptibility by the relation

$$G_n = -\frac{\nu L}{c}\chi_n'', \tag{9}$$

where G_n is the saturated single-pass fractional power gain of the nth mode and depends nonlinearly upon frequency, excitation, and power level. Similarly, we write

$$\psi_n = \frac{\nu L}{c}\chi_n', \tag{10}$$

where ψ_n is the additional round-trip phase retardation which is seen by the nth mode as a result of the insertion of the atomic medium and also depends nonlinearly upon frequency, excitation, and power level.

Although when possible the equations developed are left in terms of the general expressions G_n and ψ_n, in specific numerical calculations we consider the essence of the problem to be treated by the example of a Doppler-broadened Gaussian atomic line with homogeneous linewidth much smaller than both the axial mode interval and Doppler linewidth. For these cases, we will express the saturated gain as

$$G_n = g_n(1 - \beta E_n^3), \tag{11}$$

where g_n is the unsaturated fractional power gain per pass of the nth mode and β the saturation parameter. For the Doppler-broadened Gaussian line we have then

$$g_n = g_0\frac{Z_i\left(\frac{\nu_n - \omega}{Ku}\right)}{Z_i(0)}. \tag{12}$$

Corresponding to this, we take ψ_n to be

$$\psi_n = g_0\frac{Z_r\left(\frac{\nu_n - \omega}{Ku}\right)}{Z_i(0)}. \tag{13}$$

Here g_0 is the unsaturated line-center gain and Z_r and Z_i are the real and imaginary parts of the plasma dispersion function and are described by Lamb.[11] For vanishingly small homogeneous linewidth, (12) and (13) become g_0 times the normalized Gaussian and the Hilbert transform of the Gaussian, respectively. The parameter ω is the center frequency of the atomic line and Ku equals 0.6 times the half-power Doppler linewidth.

The single-pass power loss α_n is related to the Q of the nth mode by the expression

$$\alpha_n = \frac{\nu L}{c}\frac{1}{Q_n} \tag{14}$$

and includes both dissipative and output coupling loss (mirror transmission). In typical cases α_n is independent of n and we let $\alpha_n = \alpha$.

The time-varying loss perturbation is taken to have $\Delta\chi''$ independent of z over the length l of the perturbing element. By assuming small loss, the power loss per pass $\alpha(t)$ through this perturbing element is readily shown to be

$$\alpha(t) = W(1 + \cos\nu_m t) \tag{15}$$

where W is given by

$$W = \frac{\nu l}{c}\Delta\chi'' \tag{16}$$

and is the average loss. If the perturbing element is located such that its center is a distance z_0 from the end mirror, we obtain the self-coupling term α_a from (3)

$$\alpha_a = \frac{2W}{l}\int_{z_0-l/2}^{z_0+l/2} \sin^2\frac{(n_0+n)\pi z}{L}\,dz, \tag{17}$$

or since n_0 is very large,

$$\alpha_a = W. \tag{18}$$

Thus the self-coupling term is simply equal to the average loss introduced by the perturbation. We obtain from (4), (16), and (18) the cross-coupling term

$$\alpha_c = \frac{\alpha_a}{l}\int_{z_0-l/2}^{z_0+l/2} \sin\frac{(n_0+n)\pi z}{L}\sin\frac{(n_0+n+1)\pi z}{L}\,dz \tag{19}$$

which, again noting that n_0 is very large, yields

$$\alpha_c = \frac{L}{l}\frac{\alpha_a}{\pi}\sin\frac{\pi l}{2L}\cos\frac{z_0\pi}{L}. \tag{20}$$

For the practical case of $l \ll L$ this becomes

$$\alpha_c = \frac{\alpha_a}{2}\cos\frac{z_0\pi}{L}. \tag{21}$$

The form of (21) is analogous to that obtained by Crowell[4] for loss modulation and Harris and McDuff[9] for phase modulation. It is desirable to locate the perturbing element close to the end of the cavity so that $z_0 \approx 0$ and such that

$$\alpha_c \approx \frac{\alpha_a}{2}. \tag{22}$$

To summarize, we define the loss terms as follows: α_n is the single-pass power loss of the nth mode which results from dissipative and coupling loss not dependent on the internal perturbation; α_a is equal to the average loss per pass introduced by the perturbation; and α_c is the mode coupling term resulting from the internal perturbation. In places where all modes are assumed to have losses independent of n, we will let $\alpha_n = \alpha$. The coupling factor α_c is analogous to δ in the FM laser.[9]

IV. Conservation Conditions

We now derive conservations which result from the basic differential equations. These are similar to those of Harris and McDuff[9] for the phase modulation case and are derived in an identical manner.

Multiplying (7) by E_n, summing over n, and using the constants of the previous section, we obtain

$$\sum_n E_n\dot{E}_n = \frac{c}{2L}\Big[\sum_n (G_n-\alpha_n)E_n^2\Big] - \frac{c}{2L}\Big[\alpha_a\sum_n E_n^2 + 2\alpha_c\sum_n E_{n+1}E_n\cos(\varphi_{n+1}-\varphi_n)\Big]. \tag{23}$$

Noting that $\sum_n E_n\dot{E}_n = d/dt\,[\sum_n E_n^2/2]$, (23) can be interpreted as an expression of conservation of power; i.e., the rate of change of energy stored is equal to the net power generated or absorbed in all modes. We see that, in general, the loss perturbation always absorbs power from the system. However in a hypothetical ideal system wherein all E_n's are equal, all $\varphi_{n+1} - \varphi_n = \pi$, and such that $\alpha_c = \frac{1}{2}\alpha_a$ (modulator at the end of the optical cavity); we see that the parametric term on the right side of (23) is identically equal to zero and contributes no net loss. We shall see later that under various operating conditions the coupled system tries to adjust itself toward this ideal situation. This situation corresponds to the physical picture offered by Crowell[4] of the light pulse going through the perturbing element at that instant of time when its attenuation is zero.

Applying a similar procedure to (6), we obtain the reactive conservation condition

$$\sum_n \dot{\varphi}_n E_n^2 = \sum_n \Big(n\,\Delta\nu - \frac{c}{2L}\psi_n\Big)E_n^2. \tag{24}$$

Solutions of (6) and (7) which give a nonbeating equilibrium point have $\dot{E}_n = 0$ and all $\dot{\varphi}_n$ equal to some constant. In such cases (24) yields

$$\dot{\varphi} = \frac{\sum_n (n\,\Delta\nu - c/2L\,\psi_n)E_n^2}{\sum_n E_n^2}. \tag{25}$$

The absolute oscillation frequency of the nth mode is $\Omega_n - n\,\Delta\nu + \dot{\varphi}$ and is thus determined when relative mode amplitudes are known.

V. Dyadic Expansion of Steady-State Equations

In this section we develop basic relationships between mode amplitudes and phases for the nonbeating steady-state case. These equations are used later in developing an iterative procedure for determining amplitudes and phases exactly and in calculating the minimum modulator drive that will cause phase locking. The equations are also useful in evaluating the linear approximate solutions obtained by others and in obtaining approximate solutions to the nonlinear problem.

We are interested in solutions of (6) and (7) which have $\dot{E}_n = 0$ and $\dot{\varphi}_n$ equal to a constant independent of n. Equations (6) and (7) become

$$E_{n+1}\sin(\varphi_{n+1}-\varphi_n) - E_{n-1}\sin(\varphi_n-\varphi_{n-1}) = -E_n\Big[\dot{\varphi}\frac{2L}{c\alpha_c} - n\,\Delta\nu\frac{2L}{c\alpha_c} + \frac{\psi_n}{\alpha_c}\Big] \tag{26}$$

and

$$E_{n+1}\cos(\varphi_{n+1}-\varphi_n) + E_{n-1}\cos(\varphi_n-\varphi_{n-1}) = E_n\Big[\frac{G_n-\alpha-\alpha_a}{\alpha_c}\Big]. \tag{27}$$

We solve (26) for relative phase angles and treat the rest of the quantities in the equation as known. Proceeding similarly as in the case of phase modulation,[9] we construct a Green's dyadic $\mathcal{G}_{n,q}$ such that

$$E_{n+1}\mathcal{G}_{n+1,q} - E_{n-1}\mathcal{G}_{n,q} = \delta_{n,q}, \tag{28}$$

where $\delta_{n,q}$ is the Kronecker delta, and introduce the boundary condition that $\mathcal{G}_{n,q} = 0$ at $n = +\infty$. We find

$$\mathcal{G}_{n,q} = \frac{-E_n}{E_n E_{n-1}} \qquad n \leq q$$
$$= 0 \qquad n > q. \tag{29}$$

From (26), the equation for the relative phase is then

$$\sin(\varphi_n - \varphi_{n-1}) = -\sum_{q=-\infty}^{\infty} \mathcal{G}_{n,q}\left[\dot{\varphi}\frac{2L}{c\alpha_c} - q\,\Delta\nu\frac{2L}{c\alpha_c} + \frac{\psi_q}{\alpha_c}\right]E_q$$
$$\sin(\varphi_n - \varphi_{n-1}) = \frac{1}{E_n E_{n-1}}\frac{1}{\alpha_c}\sum_{q=n}^{\infty}\left[\dot{\varphi}\frac{2L}{c} - q\,\Delta\nu\frac{2L}{c} + \psi_q\right]E_q^2. \tag{30}$$

Similar to the case of phase modulation,[9] there is a complementary form of (30) which sums over q from $-\infty$ to $n-1$. The equivalence of the two forms is assured by the reactive conservation condition (24). Equation (30) is one of the principal results of this section.

A useful identity is now obtained from (27). First, it is rewritten in the form

$$E_{n+1} - \left(\frac{\alpha + \alpha_a}{\alpha_c}\right)E_n + E_{n-1} = -\frac{G_n}{\alpha_c}E_n + E_{n+1}\cdot[1 + \cos(\varphi_{n+1} - \varphi_n)] + E_{n-1}[1 + \cos(\varphi_n - \varphi_{n-1})]. \tag{31}$$

If we define a Green's dyadic

$$\mathcal{G}_{n+1,q} - \left(\frac{\alpha + \alpha_a}{\alpha_c}\right)\mathcal{G}_{n,q} + \mathcal{G}_{n-1,q} = \delta_{n,q} \tag{32}$$

with the boundary conditions $\mathcal{G}_{n,q} = 0$ at $n = \pm\infty$, we obtain the identity

$$E_n = \sum_{q=-\infty}^{\infty}\mathcal{G}_{n,q}\left\{\frac{-G_q}{\alpha_c}E_q + E_{q+1}[1 + \cos(\varphi_{q+1} - \varphi_q)] + E_{q-1}[1 + \cos(\varphi_q - \varphi_{q-1})]\right\}. \tag{33}$$

We choose these boundary conditions because we are interested in a solution with mode amplitudes approaching zero at $|n|$ large. By solving (32) we get

$$\mathcal{G}_{n,q} = \frac{-1}{2\sqrt{\left(\frac{\alpha + \alpha_a}{2\alpha_c}\right)^2 - 1}}\cdot\left[\left(\frac{\alpha + \alpha_a}{2\alpha_c}\right) - \sqrt{\left(\frac{\alpha + \alpha_a}{2\alpha_c}\right)^2 - 1}\right]^{|n-q|}. \tag{34}$$

The identity (33) becomes

$$E_n = \frac{1}{\sqrt{(\alpha + \alpha_a)^2 - 4\alpha_c^2}}\cdot\sum_{q=-\infty}^{\infty}\left[\frac{\alpha + \alpha_a}{2\alpha_c} - \sqrt{\left(\frac{\alpha + \alpha_a}{2\alpha_c}\right)^2 - 1}\right]^{|n-q|}\mu_q \tag{35}$$

with

$$\mu_q = G_q E_q - \alpha_c E_{q+1}[1 + \cos(\varphi_{q+1} - \varphi_q)] - \alpha_c E_{q-1}[1 + \cos(\varphi_q - \varphi_{q-1})]. \tag{36}$$

Equation (35) is the second important result of this section.

To gain a better understanding of (35), consider the case when $\Delta\nu$ and ψ_n are small and/or α_c is large. It will be seen in Section VII, for this case, that the relative phase angles are approximately equal to π. Equation (35) becomes

$$E_{n\,\text{Approximate}} = \frac{1}{\sqrt{(\alpha + \alpha_a)^2 - 4\alpha_c^2}}\cdot\sum_{q=-\infty}^{\infty}\left[\frac{\alpha + \alpha_a}{2\alpha_c} - \sqrt{\left(\frac{\alpha + \alpha_a}{2\alpha_c}\right)^2 - 1}\right]^{|n-q|}G_q E_q. \tag{37}$$

Furthermore, consider the case in which there is gain in only the center mode, i.e., only $G_0 \neq 0$, which in this case yields

$$E_{n\,\text{One mode}} = \frac{G_0 E_0}{\sqrt{(\alpha + \alpha_a)^2 - 4\alpha_c^2}}\left[\left(\frac{\alpha + \alpha_a}{2\alpha_c}\right) - \sqrt{\left(\frac{\alpha + \alpha_a}{2\alpha_c}\right)^2 - 1}\right]^{|n|}. \tag{38}$$

DiDomenico[2] treated the one-mode line in his linearized work and obtained an equation analogous to (38). In this case where losses are assumed independent of n, the linearized treatment gives correct relative amplitudes while the saturation of the center mode sets the scale. One then obtains the following interpretation of (37): the identity is analogous to a homogeneous integral equation in which the nth-mode amplitude is given by a convolution of the single-mode "response" and the product of the saturated gain profile and mode amplitude profile.

VI. Iterative Technique for Solving the Steady-State Problem

If the relative phase angles $\varphi_n - \varphi_{n-1}$ are not exactly π, then small additional terms are present in (36). In this case mode amplitudes and phases may be obtained by an iterative procedure. One begins by making a selection of relative mode amplitudes and phases. The power conservation condition (23) is then used to find the level of oscillation. The mode phases and scaled amplitudes are inserted into (35) and new values $E_n^{(1)}$ are calculated. These new values are used in (25) to calculate the frequency shift $\dot{\varphi}^{(1)}$ of the coupled oscillation. Next the values $E_n^{(1)}$ and $\dot{\varphi}^{(1)}$ are used in (30) to calculate the new relative angles $(\varphi_n - \varphi_{n-1})^{(1)}$. Although not uniquely specified by (30), these angles are taken to be in the second or third quadrant. This agrees with the direct numerical solution of (6) and (7) and, as can be seen from (23), angles in these quadrants cause the loss represented by α_c to subtract from that due to α_a and thereby to reduce the net modulator loss. Finally the new values

$E_n^{(1)}$ and $(\varphi_n - \varphi_{n-1})^{(1)}$ are used in (35) and the cycle is repeated until the process converges.

Unfortunately, this iterative procedure converges relatively slowly. Although (35) includes saturated gain and therefore, in effect, includes the conservation condition (23), the convergence is improved if (23) is used to set the scale each time before repeating the iteration cycle. The iterative procedure is recommended only when α_c is near its optimum value and larger (when $\alpha_c \gtrsim g_0 - \alpha$). In this case, the use of free-running mode amplitudes (with a "tailing off" added on either side) and all relative phase angles equal to π as starting values gives a convergent answer in about ten iterations. This requires about one fourth as much computer time as the direct numerical solution of (6) and (7).

VII. Variation of α_c at Constant Modulator Frequency

In this section we present the results of numerical analysis for a particular set of laser constants. We assume a Doppler-broadened Gaussian atomic line with a homogeneous linewidth much smaller than the axial mode interval and take g_n and ψ_n to be given by (12) and (13). Using the definitions of Section III, we take $g_0 = 0.075$, $\alpha = 0.070$, and assume an axial mode interval of 0.1 Ku. This corresponds to a ratio of Doppler width to mode spacing of 16.67 and gives five free-running modes above threshold. In this and the following section, the modulator is taken to be at the end of the cavity so that the coupling term α_c is equal to one-half the average single-pass loss α_a through the modulator. In specifying the detuning of the modulator drive, we include the linear part of ψ_n in the definition of the mode spacing $\Delta\Omega$.[3] Mode amplitudes, phases, and frequencies were obtained by direct digital computer solution of (6) and (7) using a fourth-order Runge–Kutta method. The equations were programmed for 21 modes ($n = -10$ to $n = +10$) and were run until a steady-state solution to three decimal places was reached. Unless otherwise noted in the following, the $n = 0$ mode was taken to be at line center.

In Fig. 1 we show laser mode amplitudes and the resultant variation of total laser intensity with time at the modulator position. Since the plot is versus $\nu_m t$, it gives directly a picture of spike position relative to phase of the modulator drive. In Fig. 1(a) we show the results for $\alpha_c = 0.00008$ and $\Delta\nu/\Delta\Omega = -0.00003$. As will be seen in Section IX this detuning is approximately the optimum value at low modulator drive levels. The mode amplitudes are essentially the free-running values while the relative phase angles (not shown) vary widely within the range from 90° to 270°. The resultant intensity waveshape has large ripple and a relatively wide spike. This

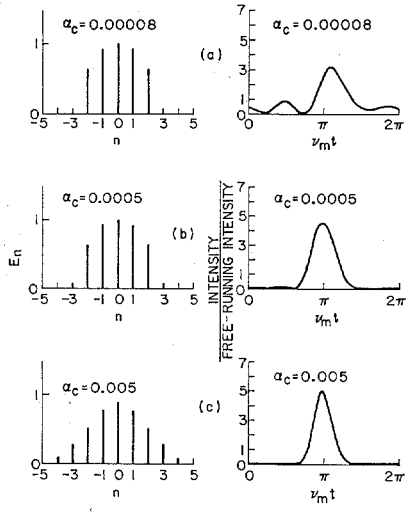

Fig. 1. Laser mode amplitudes and intensity pulseshape at constant detuning and variable α_c: $g_0 = 0.075$; $\alpha = 0.070$; $\Delta\Omega = 0.1\ Ku$; $\Delta\nu = -0.00003\ \Delta\Omega$ (five modes free-running).

operating point is very close to the condition at which phase locking just barely occurs. In Fig. 1(b) we show the results at the same modulator frequency but at a higher drive level, $\alpha_c = 0.0005$. This could be classed as an intermediate region where mode amplitudes are still close to free-running but phase angles have become more uniform. The resultant improvement in spike shape is obvious. Finally, in Fig. 1(c) we show results at very nearly the optimum drive level, $\alpha_c = 0.005$. The mode amplitudes are very close to Gaussian while the angles are close to 180°. This results in a Gaussian-shaped pulse with zero ripple between pulses. A further increase in α_c broadens the linewidth of the Gaussian mode envelope and thereby reduces both the average power output and the half-power pulsewidth.

We find that when the $n = 0$ mode is at line center, the mode amplitudes and relative phase angles are symmetrical about $n = 0$. If the center mode is off line center, at large α_c relatively little happens. The envelope of the mode amplitude profile remains the same. Individual mode amplitudes change as they shift position beneath this envelope. The resultant phase angles become somewhat asymmetrical and, as expected from (25), there is a slight shift in frequency of the coupled oscillation, i.e., all mode frequencies shift from their assumed values by an amount $\dot{\varphi}$. There is only a slight reduction in laser power and spike height, and the overall results are not significant. In contrast, if α_c is near the minimum value that will cause phase locking, as in Fig. 1(a), the effects of the center mode moving off line center are quite severe. Relative phase angles change greatly and a nonsteady-state situation may occur. This case is considered further in Section IX.

Figure 2 shows the variation of the peak pulse intensity as α_c is changed. The detuning and laser constants remain as in Fig. 1. For comparison we show the performance of an identical laser having an internal phase perturbation driven at a frequency equal to its axial mode interval (i.e., in the region termed "phase-locked"[8]–[10]). The

[3] The function Z_r of (13) can be expanded in the power series[12]

$$Z_r(\zeta) = 2\zeta\left(1 - \frac{2\zeta^2}{3} + 4\frac{\zeta^4}{15} - \frac{8\zeta^6}{105} + \cdots\right).$$

We define $\Delta\nu$ with respect to the mode spacing that would be obtained if only the leading term of the expansion were present.

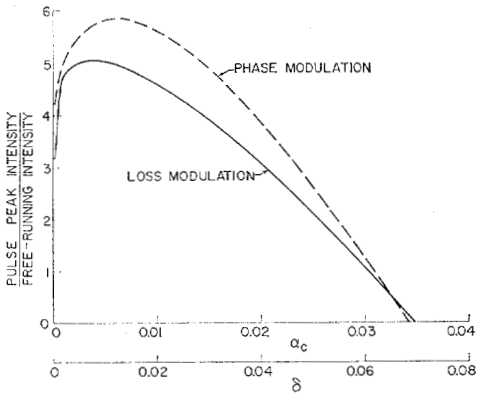

Fig. 2. Pulse peak intensity versus perturbation level at constant detuning: $g_0 = 0.075$; $\alpha = 0.070$; $\Delta\Omega = 0.1\ Ku$; $\Delta\nu = 0$ for phase modulation; $\Delta\nu = -0.00003\ \Delta\Omega$ for loss modulation (five modes free-running).

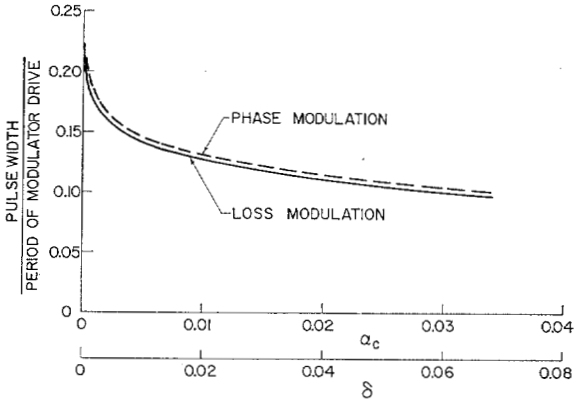

Fig. 3. Pulsewidth versus perturbation level at constant detuning: $g_0 = 0.075$; $\alpha = 0.070$; $\Delta\Omega = 0.1\ Ku$; $\Delta\nu = 0$ for phase modulation; $\Delta\nu = -0.00003\ \Delta\Omega$ for loss modulation (five modes free-running).

quantity δ is the peak single-pass phase retardation of the perturbing element.[4] For both types of modulation we note an initial increase in spike amplitude at low modulation levels as the relative phase angles improve with increasing drive. At high levels of drive, a decrease in spike amplitude occurs with eventual extinguishing of the laser. In loss modulation the decrease at higher drive occurs because of the nonzero modulator loss (proportional to drive level) and because energy is coupled from modes having net gains to modes with net loss. In phase modulation only the latter effect occurs. The optimum peak intensity obtained with loss modulation is about twenty percent below that obtained with phase modulation. Similar results are obtained for other laser constants.

In Fig. 3 we show variation in pulsewidth under the same conditions as Fig. 2. The initial rapid decrease in pulsewidth is due to rapidly improving relative phase angles while the slow continued decrease is a result of the slight broadening of the oscillating linewidth at high drive levels.

VIII. Variation of Modulator Frequency at Constant α_c

In this section we consider the effects of varying the modulator drive frequency over the range wherein steady-state locking occurs. The height, width, and position of the laser pulses are shown in Figs. 4, 5, and 6, respectively. The results were obtained by direct numerical solution of (6) and (7).

Several interesting points are illustrated by these curves. First, the range of $\Delta\nu$ over which phase locking occurs varies greatly with modulator drive. We will see in Section IX that this range approaches zero as α_c is decreased to its threshold value. Second, there is an optimum frequency which is relatively independent of drive level.[5] As the frequency is changed from this value, the pulse performance is degraded in every respect, i.e., the peak value decreases, the pulse widens slightly, and the phase of the peak varies relative to modulator drive.

These results are consistent with the equations developed in Sections IV and V and can be explained using them. The relative phase angles are dependent on detuning and mode pulling as shown by (30) and depart farther and farther from π as detuning is changed from its optimum value. In a multimode laser, α_c is typically much smaller than the gain G_q of the oscillating modes so that the dominant part of μ_q in (35) and (36) is the G_qE_q term. Thus the *relative* mode amplitudes are approximately independent of phase angles and therefore detuning. The *scale* of mode amplitudes is strongly dependent upon phase angles, however, as is clearly evident from (23). If the mode amplitudes are written in the form $E_n = ke_n$ where $\sum_n e_n^2 = 1$, (23) becomes

$$\sum_n E_n^2 = k^2 = \frac{1}{\beta}\frac{\sum_n (g_n - \alpha)e_n^2 - \alpha_a \sum_n e_n^2 - 2\alpha_c \sum_n e_{n+1}e_n \cos(\varphi_{n+1} - \varphi_n)}{\sum_n g_n e_n^4}. \tag{39}$$

Thus the average laser power, which is proportional to $\sum_n E_n^2$, is sensitive to changes in $(\varphi_{n+1} - \varphi_n)$, especially at the larger values of α_c. If $\alpha_a \gtrsim (g_0 - \alpha)$, we see that the laser is extinguished as the relative angles depart greatly from π and, therefore, is extinguished at large detunings. If α_a is smaller than the excess gain, the laser is not extinguished but, as will be seen, ceases to be phase locked at large detunings.

Since the pulsewidth changes little as $\Delta\nu$ is varied, the average power follows very nearly the same shaped curve as does peak power in Fig. 4. For a case corresponding to α_a greater than excess gain, Crowell[4] observed experimentally such a variation in average power as the cavity resonant frequency was changed (equivalent to detuning the modulator drive). He also observed a shift in spike position similar to Fig. 6.

[4] The relative alignment of the scales of α_c and δ is such that on a single pass basis the two modulators transfer the same amount of power into adjacent sidebands.

[5] The fact that this frequency differs from zero is a consequence of the definition of axial mode interval. In comparing with experiments, a consistent definition must be used.

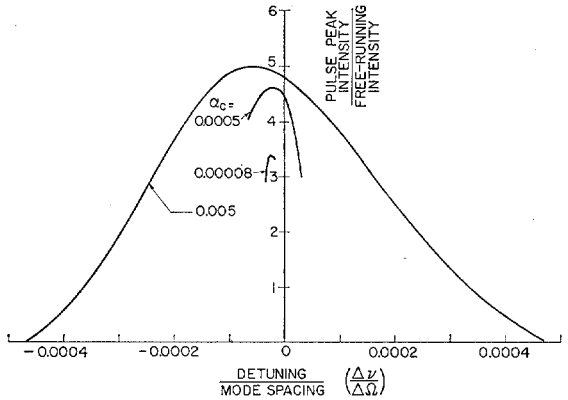

Fig. 4. Pulse peak intensity versus detuning at constant α_c: $g_0 = 0.075$; $\alpha = 0.070$; $\Delta\Omega = 0.1\ Ku$ (five modes free-running).

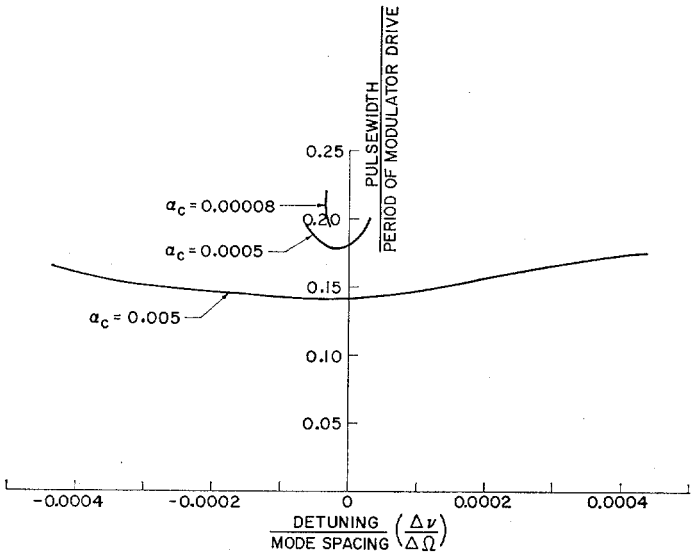

Fig. 5. Pulsewidth versus detuning at constant α_c: $g_0 = 0.075$; $\alpha = 0.070$; $\Delta\Omega = 0.1\ Ku$ (five modes free-running).

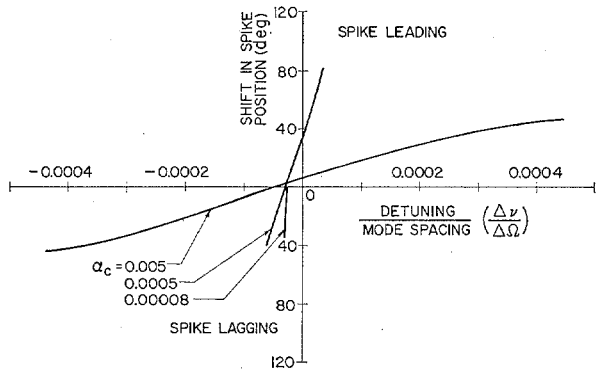

Fig. 6. Pulse relative phase versus detuning at constant α_c: $g_0 = 0.075$; $\alpha = 0.070$; $\Delta\Omega = 0.1\ Ku$ (five modes free-running).

IX. Threshold of Phase Locking

Since in practice the strength of an intracavity loss perturbation may be limited, it is important to know the minimum perturbation that will phase lock a multimode laser. We find that the mode pulling of the active medium specifies such a minimum.

At low modulator drive one expects the parametric terms (right-hand side) in (7) to have negligible effect and the mode amplitudes, therefore, to be approximately equal to their free-running values. This was seen to be the case in Fig. 1(a). By contrast, because the atomic mode pulling term χ_n' depends nonlinearly on n, it is impossible to have a steady-state solution ($\dot{\varphi}$ = constant) to (6) in which the parametric term is neglected. In the absence of the perturbation, the modes are at their free-running frequencies and, therefore, unequally spaced. The perturbation has to pull the modes until their frequency spacing is that of the modulator drive.

Assuming mode amplitudes to be the free-running values, the parametric pulling term then depends upon α_c and the relative phase angles as seen in (6). As α_c is reduced, the sine terms must increase and eventually a limit is reached when one of them becomes ± 1. For a further decrease in α_c a steady-state solution may no longer be obtained, and a beating of mode amplitudes and phases results.

With mode amplitudes known, (30) affords a convenient means to calculate the limiting value of α_c. Each relative phase angle sets a requirement, $\alpha_c \geq (\alpha_c)_n$, where the $(\alpha_c)_n$ are found by letting $\sin(\varphi_n - \varphi_{n-1}) = \pm 1$ in (30); i.e.,

$$(\alpha_c)_n = |Y_n(\Delta\nu)| \tag{40}$$

where we have defined

$$Y_n(\Delta\nu) = \frac{1}{E_n E_{n-1}} \sum_{q=n}^{\infty} \left[\dot{\varphi}\frac{2L}{c} - q\,\Delta\nu\frac{2L}{c} + \psi_q \right] E_q^2. \tag{41}$$

The largest such value of α_c is the minimum that will be sufficient to cause phase locking of all the modes at the given $\Delta\nu$. In Fig. 7 we show a plot of the minimum value of α_c that will cause phase locking versus $\Delta\nu/\Delta\Omega$ for a case having $g_0 = 0.085$, $\alpha = 0.070$, and $\Delta\Omega = 0.1\ Ku$. This case is identical to that considered in Sections VII and VIII except that gain has been increased to give nine modes free-running. The curve is seen to be made up of straight line segments resulting in a sharp minimum at an optimum detuning. We define threshold as this minimum value of α_c.

If the center mode is at line center, there exists a simple procedure for determining the threshold value of α_c and the optimum detuning. The quantities $Y_n(\Delta\nu)$, defined by (41), have a linear dependence upon $\Delta\nu$. If these straight lines are plotted in the $[Y_n, \Delta\nu/\Delta\Omega]$ plane, it is possible to verify that they always fall in the relative positions of Fig. 8; i.e., they intersect below the $\Delta\nu/\Delta\Omega$ axis and the Y_1 line lies above the others in the upper half plane.[6] As noted above, the smallest value of α_c that will phase lock the modes at a given $\Delta\nu$ is equal to the largest $|Y_n|$ at that $\Delta\nu$. From the geometry of Fig. 8, this largest value falls somewhere along the $n = 1$ line. Therefore the threshold point is located at the intersection of the $n = 1$ line and the particular image

[6] Only the $n > 0$ straight lines are shown since $(\varphi_1 - \varphi_0) = (\varphi_0 - \varphi_{-1})$, $(\varphi_2 - \varphi_1) = (\varphi_{-1} - \varphi_{-2})$, etc., when the center mode is at the center of a symmetrical gain profile.

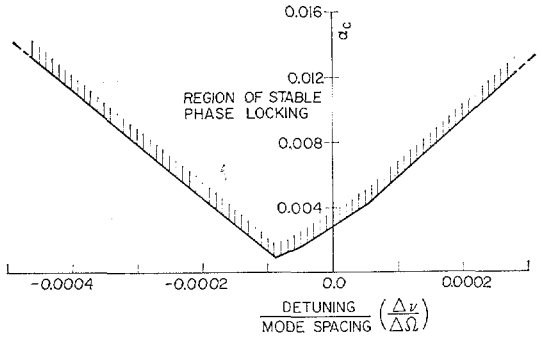

Fig. 7. Value of α_c necessary to cause phase locking versus detuning: $g_0 = 0.85$; $\alpha = 0.070$; $\Delta\Omega = 0.1\ Ku$ (nine modes free-running).

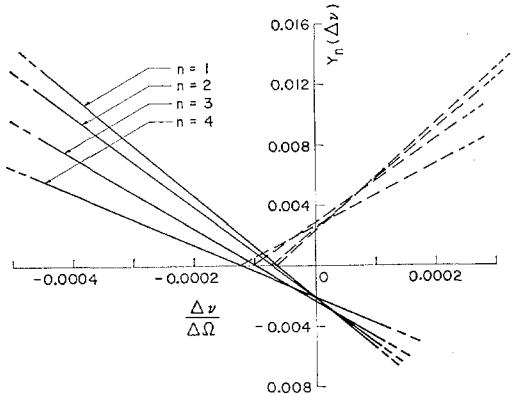

Fig. 8. $Y_n(\Delta\nu)$ versus detuning: $g_0 = 0.085$; $\alpha = 0.070$; $\Delta\Omega = 0.1\ Ku$ (nine modes free-running).

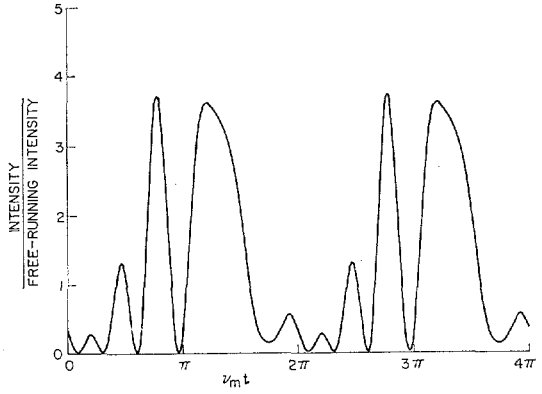

Fig. 9. Output intensity versus time at threshold of locking: $g_0 = 0.085$; $\alpha = 0.070$; $\Delta\Omega = 0.1\ Ku$ (nine modes free-running).

of the other lines (shown dashed) that gives the largest value of Y_1.

At the threshold point in Figs. 7 and 8, $(\varphi_1 - \varphi_0) = \pi/2$ and $(\varphi_4 - \varphi_3) = 3\pi/2$ while the other angles fall between these two extremes (in the second and third quadrants). Since at threshold the relative phase angles vary widely, it is expected that output pulseshapes will be greatly distorted. Figure 9 shows the output intensity resulting from amplitudes and phases calculated at the above threshold point. We note sidelobes which have intensities comparable to the main spike. This might explain the multiple spiking which has been observed experimentally.[4]

The effects of detuning at low perturbations can be understood more clearly by reference to Fig. 8 since, at a given α_c, $\sin(\varphi_n - \varphi_{n-1})$ is directly proportional to $Y_n(\Delta\nu)$; i.e., by using (41), then (30) can be written

$$\sin(\varphi_n - \varphi_{n-1}) = \frac{1}{\alpha_c} Y_n(\Delta\nu). \tag{42}$$

At $\alpha_c = 0.004$ then, for example, steady-state locking is to be expected as $\Delta\nu$ is made more and more negative until the uppermost line ($n = 1$) rises above the point, $Y_n = 0.004$. Here $(\varphi_1 - \varphi_0)$ becomes $\pi/2$ and steady-state locking ceases. Since the lines are widely spaced at this point, the other relative angles are considerably different and the pulse becomes more and more distorted as this nonsteady-state condition is approached. In contrast, as $\Delta\nu$ is *increased* from the value at threshold the angles become more and more nearly equal since the lines are converging. The $n = 3$ line first rises above $Y_n = 0.004$ [therefore, $(\varphi_3 - \varphi_2)$ is the limiting angle] but at that point the other relative angles are approximately equal to $(\varphi_3 - \varphi_2)$. As this nonsteady-state condition is approached, the expected pulseshape is actually improving. Hargrove, Fork, and Pollack[1] noted such a contrast in behavior with detuning as the extremes of the locking range were approached.

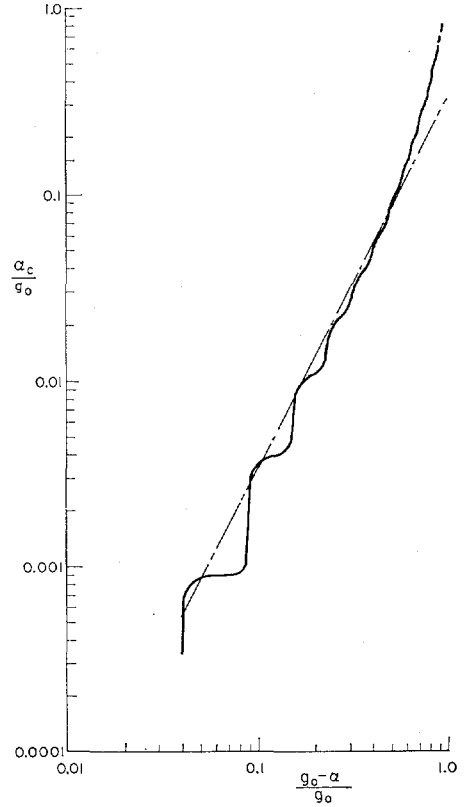

Fig. 10. Variation of threshold value of α_c with excess gain: $\Delta\Omega = 0.1\ Ku$.

In Fig. 10 we show the calculated locking threshold α_c versus excess gain at the same mode spacing, $\Delta\Omega = 0.1\ Ku$, as in the previous figures. The ripple in the curve at low excess gain is a result of the change of the number of free-running modes as the gain is increased. At the left end the curve starts with five modes free-running

and each successive hump corresponds to two additional modes coming above the free-running threshold. We also find that the threshold α_c changes as the center mode moves off line center. If we determine the α_c necessary to insure locking *regardless* of the position of the center mode, we find that the space between humps is filled in and the curve becomes very nearly the straight line shown dashed in Fig. 10. At large $(g_0 - \alpha_n)$ the mode amplitudes are affected by the larger α_c and depart from their free-running values. It becomes easier to phase lock the modes than is predicted by assuming free-running amplitudes. This lowers the curve to the dashed line in Fig. 10 at large $(g_0 - \alpha_n)$. In general, we find that the threshold α_c varies approximately as the square of excess gain.

X. Gain in a Single Mode

We have seen that the internal perturbation not only locks the existing free-running modes but also strongly affects their amplitudes and produces nonzero amplitudes where modes were previously below threshold. As an extreme example, this section considers the situation where the atomic gain profile is so narrow that only one laser mode has gain. Since their effects are similar to the multimode case, mode pulling and detuning will not be considered. Mode amplitudes were given by (38) which is rewritten here as

$$E_n = E_0\, r^{|n|}, \tag{43}$$

where

$$r = \left[\frac{\alpha + \alpha_a}{2\alpha_c} - \sqrt{\left(\frac{\alpha + \alpha_a}{2\alpha_c}\right)^2 - 1}\right], \tag{44}$$

and E_0 is determined from the power conservation requirement

$$G_0 = \sqrt{(\alpha + \alpha_a)^2 - 4\alpha_c^2}. \tag{45}$$

If inhomogeneous saturation of the form of (11) is assumed, then (45) gives

$$E_0 = \sqrt{\frac{1}{\beta}\left[1 - \frac{1}{g_0}\sqrt{(\alpha + \alpha_a)^2 - 4\alpha_c^2}\right]}. \tag{46}$$

The laser intensity has a time dependence given by[9]

$$W(t) = \tfrac{1}{2}\sum_s \sum_n E_n E_{n+s} \cos\left(s\nu_m t + \varphi_{n+s} - \varphi_n\right). \tag{47}$$

For the one active mode line, we substitute (43) into (47), use standard geometric sum formulas and obtain

$$\underset{\text{one mode}}{W(t)} = \frac{E_0^2}{2}\sum_s r^{|s|}\left(|s| + \frac{1 + r^2}{1 - r^2}\right)\cos\left(s\nu_m t + \pi\right). \tag{48}$$

The resultant output intensity has peak and minimum values given by

$$\begin{aligned} \underset{\text{one mode}}{W(t)}\Big|_{\text{peak}} &= \frac{E_0^2}{2}\left(\frac{1 + r}{1 - r}\right)^2; \qquad \nu_m t = \pi, 3\pi, 5\pi, \cdots \\ \underset{\text{one mode}}{W(t)}\Big|_{\text{min}} &= \frac{E_0^2}{2}\left(\frac{1 - r}{1 + r}\right)^2; \qquad \nu_m t = 0, 2\pi, 4\pi, \cdots . \end{aligned} \tag{49}$$

Although the scale of $W(t)$ depends on E_0 and hence upon the gain, the shape of the curve depends only upon r and therefore upon α_c/α (we are still assuming (22) to be true). Normalized plots of laser intensity from (48) are shown in Fig. 11 at several values of α_c/α. At higher modulator drive levels the result is a spiking output which can be as peaked as that of a multimode laser.[7]

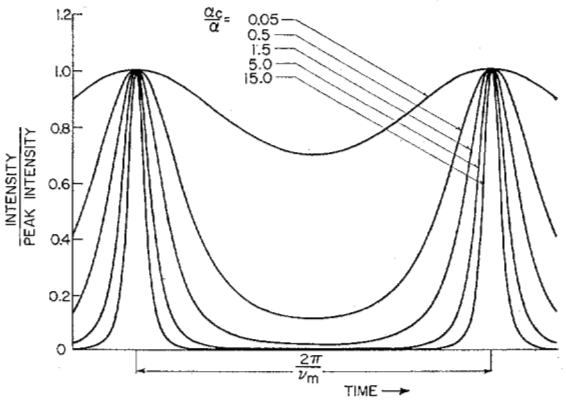

Fig. 11. Normalized intensity versus time for an atomic line having gain in only one mode.

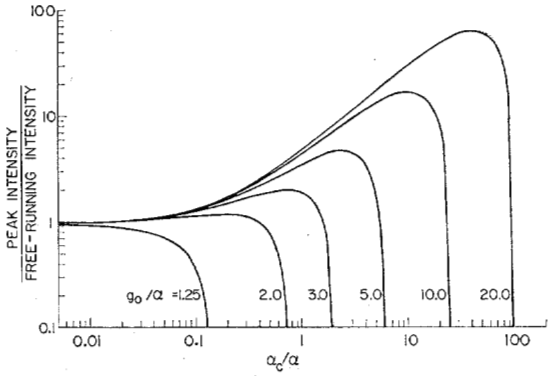

Fig. 12. Pulse peak intensity versus α_c/α for an atomic line having gain in only one mode.

The peak intensity of the spike can be many times the free-running intensity of the single mode. At free running we have

$$g_0(1 - \beta E_0^2) = \alpha. \tag{50}$$

Solving (50) for free-running intensity and combining with (46) and (49), we get

$$\frac{W(t)_{\text{peak}}}{W(t)_{\text{free running}}} = \frac{g_0/\alpha - \sqrt{1 + 4\alpha_c/\alpha}}{g_0/\alpha - 1}\left(\frac{1 + r}{1 - r}\right)^2. \tag{51}$$

Figure 12 shows a plot of (51) versus α_c/α at several values of g_0/α. As shown, there is an optimum modulator drive which produces a spiking output having a peak

[7] In this section we are considering g_0, α_c, and α which are large enough that the small gain approximations of Section III are not always correct. We still take the equations of that section as definitions of these quantities although they may not now be exactly equal to fractional gain and/or loss per pass. For example, the exact expression for gain per pass is

$$\underset{\text{per pass}}{\text{Fractional Gain}} = \frac{I_{\text{out}} - I_{\text{in}}}{I_{\text{in}}} = e^{G_n} - 1,$$

which becomes approximately equal to G_n only at G_n small.

much larger than the free-running intensity. These values are inside the cavity; however, even if one specifies optimum coupling in each case, there can still be enhancement in useful power output of about one half the amounts shown.

We have looked at the single-mode laser under the ideal conditions where there is no detuning and where the center mode is exactly at the center of the atomic line. If the center mode is not on line center, the primary effect is to reduce the gain. Consideration of pulling of the center mode in this case requires the exact solution of (6) and (7) as in the multimode situation. The effect of detuning is similar to that of the multimode problem having $\alpha_c \gtrsim (g_0 - \alpha_n)$; i.e., detuning the modulator reduces the output until the laser is extinguished. If the $n = \pm 1$ modes have small gain (but still far below free-running threshold), the only effect is to slightly increase the power output of the laser.

XI. Approximate Solutions

In this section we consider approximations to the exact solution of (6) and (7) and discuss the linearized solutions obtained by others.

A. Approximations to Nonlinear Solutions

At small and large values of perturbation α_c and at $\Delta\nu$ small, the solution of (6) and (7) can be predicted approximately. In Section IX we considered the small perturbation case. In Table I we show a comparison of the results of an exact solution of (6) and (7) near threshold with the approximate solution obtained by taking free-running mode amplitudes and using (30) to calculate angles. The laser constants are those of the nine-mode case considered in Section IX. The values obtained are seen to be very close to the exact solution.

At larger modulator drive levels we have noted that the relative mode amplitudes are almost perfectly Gaussian. At any particular assumed linewidth of this Gaussian envelope, we can use (30) to calculate relative phase angles and then (39) to calculate the scale factor. If we follow this procedure and determine the oscillating linewidth that maximizes laser intensity, we find at small $\Delta\nu$ that the answers agree closely with the exact solution of (6) and (7). Table II shows the detailed comparison of mode amplitudes and phases at $\Delta\nu = 0$. These results were obtained using laser constants of the five-mode case of Sections VII and VIII. The agreement becomes better over a wider range of $\Delta\nu$ as α_c is increased.

B. Linearized Solutions

DiDomenico[2] first obtained an approximate solution having equal mode amplitudes and relative phase angles equal to π. Taking $\Delta\nu$ and ψ_n equal to zero and assuming all G_n equal, we note that (26) and (27) have the solution

$$\begin{aligned} \text{all } E_n &= E_0 \\ \text{all } (\varphi_n - \varphi_{n-1}) &= \theta \qquad (\textit{any value}) \\ \dot{\varphi} &= 0 \end{aligned} \tag{52}$$

TABLE I
Comparison of Exact and Approximate Solutions at Small α_c

$g_0 = 0.085$ 9 modes free-running
$\alpha_n = 0.070$ $\alpha_c = 0.00135$
$\frac{\text{Doppler width}}{\text{Mode spacing}} = 16.67$ $\Delta\nu/\Delta\Omega = -0.000088$

n	*Exact* Solution of (6) and (7)		*Approximate* Free-Running Amplitudes and (30)	
	E_n	$(\varphi_n - \varphi_{n-1})$	E_n	$(\varphi_n - \varphi_{n-1})$
0	0.974	—	1.000	—
1	0.960	134.970°	0.978	138.190°
2	0.897	160.642°	0.907	162.808°
3	0.744	192.654°	0.769	194.864°
4	0.436	222.179°	0.498	221.810°
5	0.084	217.452°	0	—
6	0.008	214.089°	0	—

TABLE II
Comparison of Exact and Approximate Solutions at Large α_c

$g_0 = 0.075$ 5 modes free-running
$\alpha_n = 0.070$ $\alpha_c = 0.005$
$\frac{\text{Doppler width}}{\text{Mode spacing}} = 16.67$ $\Delta\nu/\Delta\Omega = 0$

n	*Exact* Solution of (6) and (7)		*Approximate* Optimum Gaussian Amplitudes and (30)	
	E_n	$(\varphi_n - \varphi_{n-1})$	E_n	$(\varphi_n - \varphi_{n-1})$
0	0.990	—	0.986	—
1	0.894	185.649°	0.874	186.715°
2	0.624	187.605°	0.607	189.556°
3	0.300	190.801°	0.331	194.795°
4	0.096	194.383°	0.142	201.705°
5	0.022	198.244°	0.048	209.460°
6	0.004	202.220°	0.012	217.237°
7	0.000	205.551°	0.003	224.212°

with the value of E_0 determined from the solution of

$$G_n - \alpha = \alpha_a + 2\alpha_c \cos\theta. \tag{53}$$

Here θ can have any value insofar as the linearized equations are concerned. Only by including nonlinearities or by use of a physical argument as per Crowell[4] do we know that θ should be equal to π. We note further that this solution is only an exact solution of the linearized equations when an infinite number of modes have the same gain. For a finite number, an exact solution of the linearized equations gives nonconstant mode amplitudes except for α_c vanishingly small. But then mode pulling ψ_n cannot be neglected as has been shown.

Yariv[3] obtained a solution of the linearized equations

at $\Delta\nu \neq 0$. Taking $\dot{\varphi}$ and ψ_n equal to zero, (26) and (27) yield in this case

$$(\varphi_n - \varphi_{n-1}) = -\pi/2$$
$$G_n - \alpha = \alpha_a \tag{54}$$
$$E_n = kI_n\left(\frac{1}{\pi}\frac{\Delta\Omega}{\Delta\nu}\alpha_c\right),$$

which is Yariv's solution in our notation. Here an infinite number of modes having single-pass gain equal to single-pass loss at the assumed values of E_n is required for the answer to be an exact solution of the linearized equations. Of more importance, the linearized solution fails to simulate the real answer to the nonlinear problem. In the nonlinear case a solution with $(\varphi_n - \varphi_{n-1})$ closer to π oscillates at a higher level and is, therefore, able to negate the solution of (54). Solution (54) causes modulator loss to be high and equal to the average loss, α_a [note (23) or (39)], while in the true solution the average modulator loss is approximately zero. In other terms, the pulse produced by the I_n solution would pass through the modulator when its loss is at the average value rather than zero. In the direct numerical solution of (6) and (7) we have never observed a solution in the form of (54).

ACKNOWLEDGMENT

The authors gratefully acknowledge helpful discussions with L. Osterink and the assistance of Mrs. Cora Barry with the numerical computations.

REFERENCES

[1] L. E. Hargrove, R. L. Fork, and M. A. Pollack, "Locking of He–Ne laser modes induced by synchronous intracavity modulation," *Appl. Phys. Letters*, vol. 5, pp. 4–5, July 1964.
[2] M. DiDomenico, Jr., "Small-signal analysis of internal (coupling type) modulation of lasers," *J. Appl. Phys.*, vol. 35, pp. 2870–2876, October 1964.
[3] A. Yariv, "Internal modulation in multimode laser oscillators," *J. Appl. Phys.*, vol. 36, pp. 388–391, February 1965.
[4] M. H. Crowell, "Characteristics of mode-coupled lasers," *IEEE J. of Quantum Electronics*, vol. QE-1, pp. 12–20, April 1965.
[5] T. Deutsch, "Mode-locking effects in an internally-modulated ruby laser," *Appl. Phys. Letters*, vol. 7, pp. 80–82, August 1965.
[6] R. H. Pantell and R. L. Kohn, "Mode coupling in a ruby laser," *IEEE J. of Quantum Electronics*, vol. QE-2, pp. 306–310, August 1966.
[7] M. DiDomenico, Jr., J. E. Geusic, H. M. Marcos, and R. G. Smith, "Generation of ultrashort optical pulses by mode locking the YAlG:Nd laser," *Appl. Phys. Letters*, vol. 8, pp. 180–183, April 1966.
[8] S. E. Harris and R. Targ, "FM oscillation of the He–Ne laser," *Appl. Phys. Letters*, vol. 5, pp. 202–204, November 1964.
[9] S. E. Harris and O. P. McDuff, "Theory of FM laser oscillation," *IEEE J. of Quantum Electronics*, vol. QE-1, pp. 245–262, September 1965.
[10] E. O. Ammann, B. J. McMurtry, and M. K. Oshman, "Detailed experiments on helium–neon FM lasers," *IEEE J. of Quantum Electronics*, vol. QE-1, pp. 263–272, September 1965.
[11] W. E. Lamb, Jr., "Theory of an optical maser," *Phys. Rev.* vol. 134, pp. A1429–A1450, June 1964.
[12] B. D. Fried and S. D. Conte, *The Plasma Dispersion Function (Hilbert Transform of the Gaussian)*. New York: Academic, 1961.

Far-Infrared Electronic Transitions in Solids

ARMAND HADNI, GUY MORLOT, AND PIERRE STRIMER

***Abstract*—Two years ago at the Third Quantum Electronic Conference we showed[1] that at low temperatures there were a large number of infrared transparent crystalline matrices. These solids can be doped with other ions, and we have recently found several far-infrared electronic transitions in both pure and doped materials.[2]**

FAR-INFRARED ELECTRONIC TRANSITIONS IN PURE MATERIALS

Previous Results

TWO LINES in $PrCl_3$, two lines in PrF_3, four lines in dysprosium gallate,[3] one line in $Nd(NO_3)_3 \cdot 6H_2O$, and one line in $Sm(NO_3)_3 \cdot 6H_2O$, have been previously described and explained in terms of transitions from the ground to various higher sublevels split by the crystalline field. Figure 1 shows, as an example, the spectrum of $3Ga_2O_3 \cdot 5Dy_2O_3$, and Fig. 2 the scheme of the possible transitions.[3] The spectra of PrF_3 (Fig. 3) were obtained with powder dispersed in NaCl. They have been recently confirmed in the laboratory, with a single crystal, 2-mm thick (Fig. 3, curve 4), and at the NOLC[14] with PrF_3 powder pressed in polyethylene with an effective thickness of 65 microns.

Manuscript received August 26, 1966; revised December 12, 1966.
The authors are with the University of Nancy, Nancy, France.

Pure $ErCl_3$

There are three lines in pure $ErCl_3$ that are fairly intense (Fig. 4). Figure 5 shows the evolution of the 160-micron doublet with temperature, which is measured with a carbon bolometer attached to the sample. It is most unlikely that the room temperature 69.5-cm^{-1} line shifts to lower frequencies (67-cm^{-1}) at low temperature. In Fig. 5 there is some evidence that the 69.5-cm^{-1} line is a hot line that disappears at low temperatures, while the 67-cm^{-1} line appears, is clearly visible at 45°K, and increases when the temperature is lowered down to 20°K. The energy levels of Er^{3+} are known[4] and represented in Fig. 6; however, they correspond to Er^{3+} in $LaCl_3$